Journal of Neurochemistry

JOURNAL OF NEUROCHEMISTRY | 2014

doi: 10.1111/jnc.12734

ORIGINAL ARTICLE

Bidirectional interactions between NOX2-type NADPH oxidase and the F-actin cytoskeleton in neuronal growth cones

Vidhya Munnamalai,* Cory J. Weaver,* Corinne E. Weisheit,* Prahatha Venkatraman,* Zeynep Sena Agim,* Mark T. Quinn† and Daniel M. Suter*,‡

*Department of Biological Sciences, Purdue University, West Lafayette, Indiana, USA

†Department of Microbiology and Immunology, Montana State University, Bozeman, Montana, USA

‡Bindley Bioscience Center, Purdue University, West Lafayette, Indiana, USA

Abstract

NADPH oxidases are important for neuronal function but detailed subcellular localization studies have not been performed. Here, we provide the first evidence for the presence of functional NADPH oxidase 2 (NOX2)-type complex in neuronal growth cones and its bidirectional relationship with the actin cytoskeleton. NADPH oxidase inhibition resulted in reduced F-actin content, retrograde F-actin flow, and neurite outgrowth. Stimulation of NADPH oxidase via protein kinase C activation increased levels of hydrogen peroxide in the growth cone periphery. The main enzymatic NADPH oxidase subunit NOX2/gp91^{phox} localized to the growth cone plasma membrane and showed little overlap with the regulatory subunit p40^{phox}. p40^{phox} itself exhibited colocalization with filopodial actin bundles. Differential subcellular fractionation revealed preferential association of NOX2/gp91^{phox} and p40^{phox} with the membrane and the cytoskeletal fraction, respectively. When neurite growth was evoked with beads coated with the cell adhesion molecule apCAM, we observed a significant increase in colocalization of p40^{phox} with NOX2/gp91^{phox} at apCAM adhesion sites. Together, these findings suggest a bidirectional functional relationship between NADPH oxidase activity and the actin cytoskeleton in neuronal growth cones, which contributes to the control of neurite outgrowth.

Keywords: F-actin, growth cone, NADPH oxidase, NOX2, p40^{phox}, ROS.

J. Neurochem. (2014) 10.1111/jnc.12734

Reactive oxygen species (ROS) oxidize various molecules, including proteins, lipids, and DNA. When ROS levels are elevated, this activity can lead to oxidative stress, cell death, and aging (Sohal and Orr 2012) and contribute to several chronic and degenerative diseases, including cancer, Alzheimer's, and Parkinson's disease (Hernandes and Britto 2012; Yang *et al.* 2013). On the other hand, a growing body of literature indicates that ROS also act as important physiological signaling molecules in cell proliferation, differentiation, motility, and apoptosis (Bedard and Krause 2007; Finkel 2011). Accordingly, ROS are not only uncontrolled by-products of aerobic metabolism but are also specifically generated by NADPH oxidases, the mitochondrial respiratory chain, and lipoxygenases (Camello-Almaraz *et al.* 2006; Bedard and Krause 2007; Taddei *et al.* 2007). A tight control of cellular ROS concentration is essential to ensure specific signaling. Perturbing this redox balance can result in the aforementioned diseases.

Because of the highly reactive and short-lived nature of ROS (Winterbourn 2008), intracellular ROS signaling likely has to occur within close vicinity of the ROS source. Therefore, localized activation seems essential for ROS signaling. In non-neuronal cells, NADPH oxidases have been localized to distinct subcellular regions involved in cell

Received October 5, 2013; revised manuscript received April 2, 2014; accepted April 2, 2014.

Address correspondence and reprint requests to Dr. Daniel Suter, Department of Biological Sciences, Purdue University, 915 West State Street, West Lafayette, IN 47907-2054, USA.

E-mail: dsuter@purdue.edu

Abbreviations used: apCAM, *Aplysia* cell adhesion molecule; ASW, artificial seawater; C, central; DIC, differential interference contrast; H_2O_2, hydrogen peroxide; NOX2/gp91^{phox}, phagocytic NADPH oxidase2; p40^{phox}, cytosolic subunit of phagocytic NADPH oxidase; PDBu, phorbol 12,13-dibutyrate; PF-6, Peroxyfluor-6; P, peripheral; PKC, protein kinase C; RBI, restrained bead interaction assay; ROS, reactive oxygen species; T, transition.

adhesion and migration, including leading edge, ruffles, and focal adhesions (Ushio-Fukai 2006). Accordingly, ROS derived from NADPH oxidases have been implicated in adhesion of fibroblasts (Chiarugi *et al.* 2003) and in mig-ration of endothelial cells (Moldovan *et al.* 2000; Ushio-Fukai *et al.* 2002; Ikeda *et al.* 2005), HeLa cells (Nimnual *et al.* 2003; Kim *et al.* 2009), smooth muscle cells (Schroder *et al.* 2007; Lee *et al.* 2009), and keratinocytes (Kim *et al.* 2011). Whether ROS produced by NADPH oxidase regulate adhesive and motile processes in neurons such as growth cone protrusion, neurite outgrowth, and axon guidance is not clear.

The family of NADPH oxidases consists of seven members, which all contain a major membrane-bound flavocytochrome b_{558} enzymatic subunit but differ with respect to the composition of additional membrane-bound and cytoplasmic subunits (Bedard and Krause 2007). The first NADPH oxidase to be characterized was found in phagocytes and contained NOX2/gp91^{phox} (referred to as 'NOX2' in the remainder of this article). The fully assembled and active NOX2 complex includes the p22^{phox}, Rac1, p47^{phox}, p67^{phox}, and p40^{phox} subunits, which regulate the enzymatic activity of the NOX2 complex. NADPH oxidase family members NOX1, NOX2, NOX3, and NOX4 are expressed in different portions of the nervous system, particularly in neurons, microglia, and astrocytes (Sorce and Krause 2009; Hernandes and Britto 2012). NADPH oxidase-derived ROS have been implicated in hippocampal synaptic plasticity and memory formation (Kishida *et al.* 2006), NMDA receptor activation (Brennan *et al.* 2009), nerve growth factor-induced neuronal differentiation and neurite outgrowth of PC-12 cells (Suzukawa *et al.* 2000; Ibi *et al.* 2006), and neuronal apoptosis (Tammariello *et al.* 2000; Guemez-Gamboa and Moran 2009). On the other hand, microglial cells and proinflammatory cytokine-treated neurons release NADPH oxidase-derived superoxide leading to neuronal toxicity (Barth *et al.* 2012), as described in Alzheimer's and Parkinson's disease (Sorce and Krause 2009; Gao *et al.* 2012). We have recently reported that ROS derived from NADPH oxidases regulate F-actin organization, dynamics, and neurite outgrowth (Munnamalai and Suter 2009); however, the exact subcellular localization and interactions of NADPH oxidase with the actin cytoskeleton in neuronal growth cones have not been investigated.

Here, we report on the first localization of a NOX2-type NADPH oxidase in neuronal growth cones. NADPH oxidase inhibition with VAS2870 or celastrol resulted in reduced retrograde F-actin flow and neurite outgrowth, confirming our earlier results. NADPH oxidase activation with a protein kinase C (PKC) activator resulted in increased ROS levels in the growth cone periphery. We found that the regulatory cytosolic subunit p40^{phox} exhibited F-actin association in unstimulated growth cones and little colocalization with plasma membrane-bound NOX2. However, upon growth cone stimulation with the *Aplysia* cell adhesion molecule (apCAM), p40^{phox} and NOX2 accumulated and colocalized at adhesion sites. In summary, these findings point toward an interesting bidirectional relationship between NADPH oxidase and the actin cytoskeleton in neuronal growth cones.

Materials and methods

Aplysia bag cell neuronal culture

Aplysia bag cell neurons were plated on coverslips coated with 20 μg/mL poly-L-lysine (70–150 kD) as previously described (Lee *et al.* 2008; Suter 2011). Cells were kept in L15 medium (Invitrogen, Carlsbad, CA, USA) supplemented with artificial seawater (L15-ASW) overnight at 14°C. All reagents were from Sigma (St. Louis, MO, USA) unless otherwise specified.

Live-cell imaging and neurite outgrowth analysis

For live-cell imaging, a chamber containing *Aplysia* bag cell neurons cultured for 1 day was prepared as recently described (Lee *et al.* 2008; Suter 2011). 0.1% dimethylsulfoxide (DMSO) (vehicle control), 5 μM VAS2870 (Enzo Life Sciences, Farmingdale, NY, USA) or 5 μM celastrol (Cayman Chemical, Ann Arbor, MI, USA) dissolved in L15-ASW were sequentially applied to live neurons, while cells were observed with a 60× 1.4 NA oil objective (plus 1.5× magnification) using a Nikon TE2000 Eclipse microscope (Nikon, Melville, NY, USA; Munnamalai and Suter 2009). An OG590 long-pass red filter (Chroma Technology Corp., Bellows Falls, VT, USA) was used to eliminate shorter wavelengths harmful in live-cell imaging. Each drug was pre-incubated for 5 min before differential interference contrast images were recorded at 10-s intervals. VAS2870 and celastrol were applied for a total of 20 min. The drug was then washed out with fresh L15-ASW. For retrograde flow analysis, three kymographs of differential interference contrast time-lapse sequences were constructed from each growth cone using line scans across the peripheral (P) domain (Fig. 1; kymograph function in MetaMorph 7 software; Molecular Devices, Downingtown, PA, USA). Retrograde flow rates of individual growth cones were determined by averaging five velocity measurements from each kymograph.

Neurite outgrowth experiments were carried out similarly as previously reported (Munnamalai and Suter 2009). Neurons were imaged in L15-ASW medium 4 h after plating using a 10× phase objective. The medium was then replaced with either L15-ASW, medium containing 0.05% DMSO or 2.5 μM VAS2870 or 1 μM celastrol. Cells were incubated at 14°C for 24 h prior to a second round of imaging. Drugs were then washed out extensively with fresh L15-ASW and cells were incubated at 14°C for an additional 24 h prior to the collection of a final set of images. Total neurite length was calculated by summing the lengths of all neurites per cell. Only cells with total neurite length of $x \geq 50$ μm were included in the analysis.

NADPH oxidase immunostaining and fluorescence microscopy

After 1 day in culture, bag cell neurons were fixed with 3.7% formaldehyde/400 mM sucrose/ASW, pH 7.6 for 20 min at 20°C. Following fixation, cells were permeabilized with 0.1% saponin in fixation solution for 15 min. After three washes with phosphate-buffered saline (PBS)/0.01% saponin, cells were incubated with Alexa 488-phalloidin (1 : 100; Invitrogen) in PBS/0.01% saponin

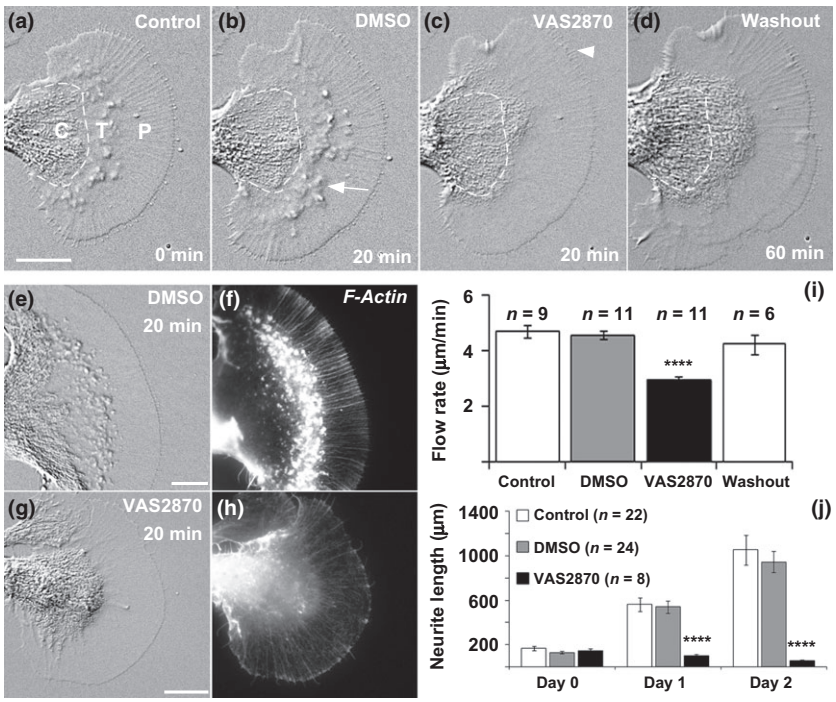

Fig. 1 NADPH oxidase inhibition reduces F-actin content in growth cones as well as neurite outgrowth. (a) Differential interference contrast (DIC) image of *Aplysia* bag cell growth cone cultured for 1 day. C domain, T zone, and P domain, as well as C domain boundary (dashed line) are indicated. (b) Treatment with 0.1% dimethylsulfoxide (DMSO) for 20 min did not affect growth cone morphology or motility. Arrow points toward T zone ruffle. (c) Treatment with 5 μM VAS2870 for 20 min caused flattening of the T zone and P domain as well as some extension of the C domain and filopodia (arrowhead). (d) Drug washout for 60 min partially reversed these effects, resulting in further growth cone protrusion. (e–h) 5 μM VAS2870 for 20 min reduced F-actin content in the T zone and P domain, including in ruffles, filopodial bundles, and lamellipodial networks. (i) NADPH oxidase inhibition by 5 μM VAS2870 resulted in reduced retrograde flow rates (Mean flow rates ± SEM; $n = 11$ growth cones; one-way ANOVA followed by Dunnett's T3 *post hoc* test; ****$p < 0.0001$). (j) NADPH oxidase inhibition by 2 μM VAS2870 between day 0 and 1 reduced neurite outgrowth irreversibly when compared with medium or DMSO-containing medium. The drug was washed out between day 1 and day 2. Mean values of total neurite length per cell ± SEM are given for different times in culture: before drug application (day 0); 24 h after drug treatment (day 1); and 24 h after drug washout (day 2). n=number of neurons; one-way ANOVA followed by Dunnett's T3 *post hoc* test; ****$p < 0.0001$. Scale bars: 10 μm.

for 20 min. Following three washes, cells were blocked with 5% bovine serum albumin in PBS/0.01% saponin for 30 min. For detection of NOX2, the rabbit anti-gp91^{phox} antibody R2085 was incubated at 1 : 500 in blocking solution for 1 h. This antibody was raised against a peptide corresponding to AA 548-560 in human gp91^{phox} (Quinn *et al.* 1989). For peptide blocking experiments (Figure S2), we used the human NOX2 548-560 peptide KQSISNSESGPRG or the corresponding *Aplysia* NOX2 peptide KHCNRFSSSESK (XP_005090645). Therefore, the NOX2 antibody was diluted at 1 : 500 in blocking solution together with the same dilution of either the human or *Aplysia* peptide (10 mg/mL stock; Genscript, Piscataway, NJ, USA) over night at 4°C before the antibody was applied to fixed neurons. A mouse anti-p40^{phox} was used at a 1 : 200 in blocking solution for 1 h at 20°C. This antibody was raised against full length human p40^{phox} (Gauss *et al.* 2002). apCAM was detected with the monoclonal antibody 4E8 diluted to 10 μg/mL in blocking solution (Suter *et al.* 1998). Following three washes, primary antibodies were detected by applying either 4 μg/mL Alexa 568 or Alexa 647 labeled goat-anti-rabbit or mouse secondary antibodies (Invitrogen) in the same blocking solution for 30 min at 20°C. Fluorescent images were acquired in 20 mM n-propyl-gallate in PBS/80% glycerol pH 8.5 on a Nikon TE2000 Eclipse microscope equipped with a 60X 1.4 NA oil (plus 1.5× magnification) objective, an X-cite 120 metal halide lamp (EXFO, Mississauga, ON, Canada), appropriate fluorescence filter sets (Chroma, Bellows Falls, VT, USA), Cascade II cooled CCD camera (Photometrics, Tucson, AZ, USA), and MetaMorph 7 software. Neuronal cell bodies were imaged by acquiring z-stacks at 10 -μm intervals on a Zeiss LSM 710 confocal microscope (Carl Zeiss Microscopy GmbH, Jena, Germany) equipped with 488, 568, and 610 nm lasers and appropriate filters.

ROS imaging

For quantitative ROS imaging, we used a hydrogen peroxide (H_2O_2)-specific fluorescent dye Peroxyfluor-6 acetoxymethyl ester Peroxyfluor-6 (PF-6) kindly provided to us by Dr. Christopher Chang, University of California, Berkeley, CA, USA (Dickinson *et al.* 2011). After 1 day in culture, growth cones were incubated for

20 min in the dark with ASW containing 5 μM PF-6 (for H_2O_2 detection) together with 250 nM Calcein Red-Orange AM (Invitrogen, Life Technologies, Grand Island, NY, USA), a cell permeable fluorescent dye used as volume marker for ratiometric imaging (Li *et al.* 2009). Three washes with ASW were performed to remove free dye. Pre-treatment images (time 0) were captured using a Nikon TE2000 Eclipse microscope using a 480-nm excitation and 535-nm emission filter for PF-6 and a 575-nm excitation and 610-nm emission filter for Calcein Red-Orange. The growth cones were then treated with ASW containing 0.1% DMSO, 0.1 μM phorbol 12,13-dibutyrate (PDBu; a protein kinase C activator), 5 μM VAS2870 or a com-bination of PDBu and VAS2870 for up to 15 min before a second set of images were taken of the same growth cones. In one set of experiments, the second image was taken 15 min after addition of VAS2870 (Fig. 2d–h). In another set, imaging was done every 30 s after addition of the drugs (Fig. 2i).

Average fluorescent intensities of both PF-6 and Calcein Red-Orange signals were measured in three regions in the growth cone periphery and then background subtracted using MetaMorph software. Each PF-6 and Calcein Red-Orange measurement was then normalized by the average DMSO control value at the same time point to correct for experimental variability. The DMSO-normalized signals were then volume corrected by dividing PF-6 values by the corresponding Calcein Red-Orange values. Volume-corrected PF-6 signals were calculated as% changes of H_2O_2 levels at specific time points by dividing each value by the time 0 value (Fig. 2i). PF-6 signals in DMSO control changed relatively little within the first 4 min (~2–5% reduction; Fig. 2i), while more significantly after 15 min of DMSO treatment (~15% reduction; Fig. 2h).

Cytochalasin treatment

To disrupt F-actin bundles only, growth cones were treated with 350 nM cytochalasin B for 5 min and then fixed and stained for F-actin, NOX2, and $p40^{phox}$ (Burnette *et al.* 2008). To strongly inhibit actin assembly in lamellipodia and filopodia, growth cones were treated with 5 μM cytochalasin B for 1 min prior to fixation and staining for F-actin, NOX2, and $p40^{phox}$ (Forscher and Smith 1988).

Biochemical fractionation

Hypotonic buffer (10 mM Tris HCl pH 7.5, 10 mM NaCl, 3 mM $MgCl_2$, 1 mM EDTA, 1 mM EGTA) was supplemented with protease inhibitors (0.5 mM Pefabloc SC Plus (Roche Diagnostics Corporation, Indianapolis, IN, USA); 1% Protease Inhibitor Cocktail), phosphatase inhibitors (10 mM NaF, 1 mM Na_3VO_4), and cytoskeletal stabilizing agents (20 μM taxol and 5 μM phalloidin). Total CNS tissue from two *Aplysia* was collected in 4 mL of ice-cold hypotonic buffer, cut into smaller pieces with dissecting scissors, and homogenized with an Omnimixer. All steps were performed at 4°C. The lysate was further homogenized with a Dounce tissue homogenizer (10 strokes) and then cleared by centrifugation at 3000 *g* for 10 min to remove nuclei and cell debris. The remaining supernatant (S1) was spun at 100 000 g in a tabletop ultracentrifuge (TLA 100.3 rotor; Beckman Coulter, Inc., Brea, CA, USA) for 1 h to separate membrane and cytoskeletal (P2) fraction from cytoplasmic (S2) fraction. The membrane and cytoskeletal fraction (P2) was resuspended in hypotonic buffer containing 1% Triton X-100 followed by centrifugation at 100 000 *g* for 1 h to separate the membrane (S3) and cytoskeletal (P3) fractions. The membrane fraction was treated with DNase 1 for 30 min to reduce the amount of membrane-associated actin cytoskeleton. The enriched membrane fraction was collected as supernatant (S4) after centrifugation at 100 000 *g* for 30 min. The cytoskeletal fraction (P3) was treated with 20 μM cytochalasin B for 30 min on ice followed by cen-trifugation at 100 000 *g* for 30 min, resulting in a supernatant (S5) containing mainly monomeric actin and a pellet (P5) containing remaining F-actin. The fractions were boiled at 70° C for 10 min, resolved on a 10% sodium dodecyl sulfate–polyacrylamide gel electrophoresis gel, and then transferred onto a polyvinylidene difluoride membrane. Following blocking with 5% non-fat dry milk in PBS, the membrane was probed with these primary antibodies: rabbit anti-actin (Sigma, A5060; 1 : 2000), rabbit anti-NOX2 (1 : 5000), and mouse anti-$p40^{phox}$ (1 : 1000) in PBS/0.05% Tween 20/0.1% non-fat dry milk. We used the secondary antibodies Alexa 680-goat-anti-rabbit and Alexa 800-goat-anti-mouse (Invitrogen) at 0.4 μg/mL in PBS/0.05% Tween 20/0.1% non-fat dry milk/0.01% sodium dodecyl sulfate, followed by detection with the Odyssey system (LI-COR Biosciences, Lincoln, NE, USA). For quantification, the integrated densities of the NOX2 and $p40^{phox}$ bands were determined for both the cytoskeletal and membrane fraction using Image J software (http://imagej.nih.gov/ij/) (Fig. 6b). The ratio of the cytoskeletal over membrane signal was determined and then averaged from three independent experiments.

Actin Coimmunoprecipitation from Aplysia CNS Lysate

Protein A-sepharose beads (#17-1279-01; GE Healthcare, Pittsburgh, PA, USA) were washed with PBS. All steps were performed at 4°C. 100 μL of washed protein A sepharose was pelleted, resuspended in 300 μL PBS containing 1 μg/μL of rabbit anti-actin antibody (Sigma, A5060), and incubated on a rotator for 1 h at 4°C. The antibody was cross-linked to protein A-sepharose using disuccinimidyl glutarate (#20593, DSG; Pierce, Thermo Fisher Scientific, Rockford, IL, USA), prepared immediately before use. DSG dissolved in DMSO was added to a final concentration of 5 mM and incubated on a rotator for 2 h. DSG was then removed by pelleting the mixture at 4000 g for 1 min. The cross-linked beads were washed twice with PBS, twice with 0.1 M glycine HCl pH 2.5 to elute any unbound antibody, and three times with PBS before beads were stored in PBS at 4°C or used for immunoprecipitation. Total CNS tissue from two *Aplysia* was collected in 4 mL of complete ice-cold lysis buffer [50 mM Tris HCl pH 7.5, 150 mM NaCl, 1 mM EGTA; 1% protease inhibitor cocktail (Cytoskeleton, Inc, Denver, CO, USA)], cut into smaller pieces with dissecting scissors, incubated in lysis buffer for 10 min on ice, and homogenized with an Omnimixer. The homogenized lysate was spun at 12 000 g for 20 min at 4°C, and the remaining supernatant was used for the immunoprecipitation. 100 μL of fresh lysate was added to 20 μL of beads with cross-linked anti-actin antibody and incubated on a rotator over night at 4°C. Following centrifugation at 4000 *g* for 1 min, the beads were washed five times with PBS and bound proteins were eluted by resuspending the beads in 75 μL PBS and 25 μL gel loading buffer and boiling at 100°C for 10 min. The boiled samples were spun as before and eluted proteins were analyzed by western blotting for both actin and $p40^{phox}$.

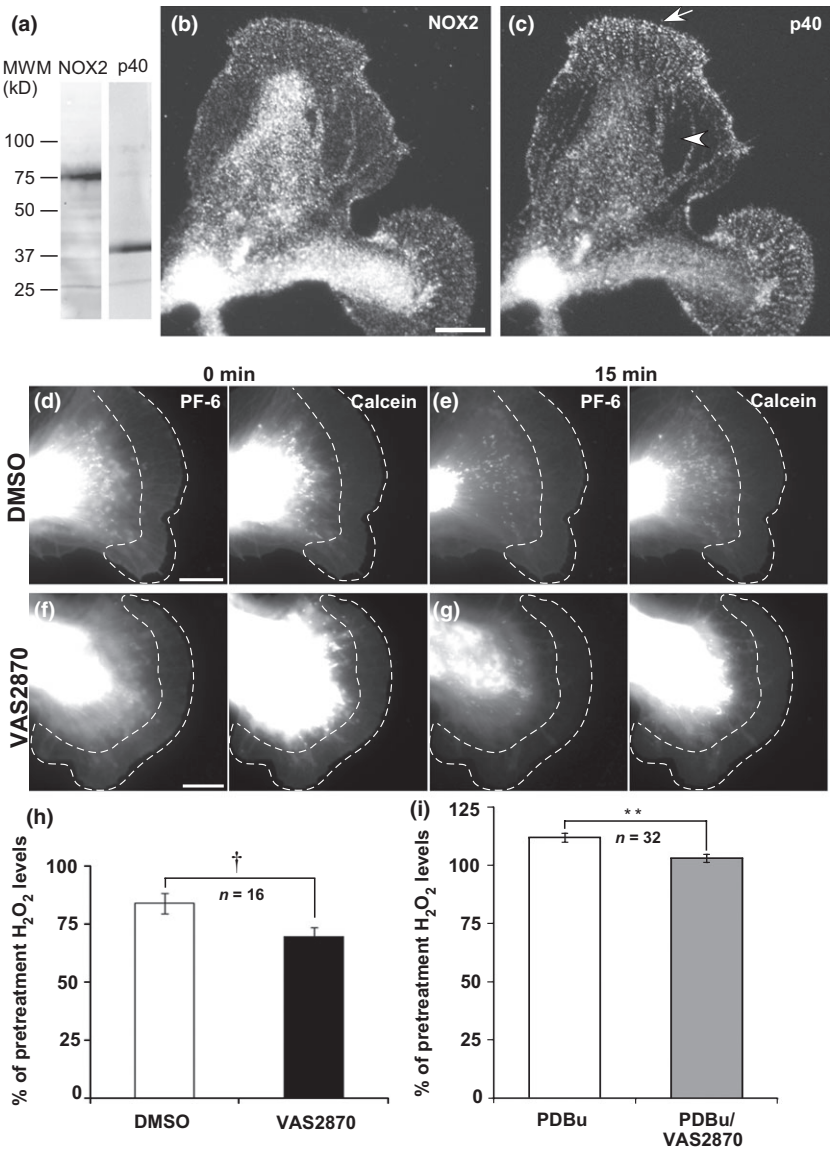

Fig. 2 Localization of a functional NOX2-type NADPH oxidase complex in *Aplysia* growth cones. (a) Western blot of *Aplysia* CNS proteins detected by NOX2 and p40 antibodies. Each antibody detects a major band at the expected molecular weights of 75 kDa and 40 kDa, respectively. (b) Immunolocalization in cultured *Aplysia* bag cell growth cones revealed homogeneous NOX2 distribution in the P domain, suggesting plasma membrane association, while the strong C domain labeling indicates vesicular association. (c) $p40^{phox}$ immunolocalization is less dense than NOX2 labeling. $p40^{phox}$ is prominent in the growth cone periphery including in filopodia (arrow). No labeling is found in very flat portions of the P domain (arrowhead). (d–g) VAS2870 lowers H_2O_2 levels in the P domain (indicated with dashed line). Peroxyfluor-6 (PF-6) signals were reduced in growth cones treated with 5 μM VAS2870 for 15 min when compared to dimethylsulfoxide (DMSO) control. Calcein red signals were used for volume correction. (h) Volume-corrected PF-6 signals after 15 min are shown as% of the pretreatment levels. DMSO: 84 ± 4%; VAS2870: 70 ± 8% (Mean values ± SEM; $n = 16$ growth cones; Student's *t*-test; †$p = 0.12$). (i) Activation of NADPH oxidase increases H_2O_2 levels. Growth cones were treated with the protein kinase C activator phorbol 12,13-dibutyrate (PDBu) (0.1 μM) to activate NADPH oxidase, or a combination of 0.1 μM PDBu and 5 μM VAS2870. Volume-corrected PF-6 signals measured after 30 s were normalized against DMSO control values and presented as% changes of pre-treatment values. PDBu increased H_2O_2 in the growth cone periphery to levels that were significantly higher than in growth cones treated with a combination of PDBu and VAS2870 (Average% changes in H_2O_2 levels ± SEM are given; $n = 32$ growth cones; one-way ANOVA followed by Dunnett's T3 *post hoc* test; **$p < 0.01$). Scale bars: 10 μm.

RBI assay

The restrained bead interaction assay (RBI) with apCAM-coated beads was performed as described (Suter *et al.* 1998, 2004). Beads were placed on the P domain of the growth cone and restrained with a glass micropipette until central (C) domain extension and protrusion of the leading edge occurred. When the C domain reached the bead, the cells were fixed and stained with NOX2 and $p40^{phox}$ antibodies.

Image processing, fluorescence intensity, and colocalization analysis

Photoshop CS3 extended (Adobe, San Jose, CA, USA) was used for image processing and making videos. Canvas X (ACD Systems of America, Inc, Miami, FL, USA) was used for final figure assembly. For quantification of NOX2 and $p40^{phox}$ signals, the average NOX2 and $p40^{phox}$ fluorescence intensities per unit area was determined in the growth cone P domain using MetaMorph 7.0, followed by background subtraction and normalization to control values in case of cytochalasin treatments. For 5 μM cytochalasin B treatments, background-subtracted fluorescence intensities of NOX2 and $p40^{phox}$ were measured in the P domain region that has been cleared from F-actin. For quantification of $p40^{phox}$ colocalization with NOX2 or F-actin, each signal was thresholded at the level of the average intensity plus 10% for a given area. After thresholding, the colocalization analysis function in MetaMorph was used to determine the% area overlap of $p40^{phox}$ with either NOX2 or F-actin or the% area overlap of NOX2 with either $p40^{phox}$ or F-actin.

Statistical analysis

Quantified data are presented as mean values ± SEM. STATISTICA 10 Academic software (StatSoft, Inc., Tulsa, OK, USA) was used for statistical data analysis. Significant differences between two conditions were determined with Student's *t*-tests if data showed normal distribution. Comparison of multiple conditions was performed with a one-way ANOVA followed by Dunnett's T3 *post hoc* test. Significance levels were labeled the following way: $*p < 0.05$; $**p < 0.01$; $***p < 0.001$; $****p < 0.0001$.

Results

NADPH oxidase inhibition negatively impacts the actin cytoskeleton and neurite outgrowth

We previously reported that lowering cytosolic ROS levels in *Aplysia* neuronal growth cones by either a general radical scavenger, α-N-tert-butyl-phenylnitrone, or by NADPH oxidase inhibition via phenylarsine oxide and apocynin resulted in reduced actin content, impaired actin dynamics, and decreased neurite outgrowth (Munnamalai and Suter 2009). Phenylarsine oxide is a potent NOX2 inhibitor, but being a vicinal dithiol-binding reagent it is not exclusively specific to NADPH oxidase (Le Cabec and Maridonneau-Parini 1995; Jaquet *et al.* 2009). Apocynin is still widely used as NADPH oxidase inhibitor; however, there is now evidence that it may act as antioxidant and require the presence of myeloperoxidase to function as a NADPH oxidase inhibitor (Heumuller *et al.* 2008; Jaquet *et al.* 2009; Wind *et al.* 2010). To confirm that our previous results were indeed caused by reduced NADPH oxidase activity, we repeated oxidase inhibition experiments with one of the most specific chemical pan-NADPH oxidase inhibitors currently available, VAS2870 (ten Freyhaus *et al.* 2006; Wind *et al.* 2010; Altenhofer *et al.* 2012).

Treatment of *Aplysia* growth cones with 5 μM VAS2870 for 20 min reduced transition (T) zone ruffling, flattened the peripheral (P) domain, caused extension of the central (C) domain and filopodial lengthening when compared to DMSO control pre-treatment (Fig. 1a–c; Video S1). These effects were partially reversible after 60 min following drug washout (Fig. 1d). NADPH oxidase inhibition significantly decreased the F-actin content in T zone ruffles, as well as in filopodial actin bundles and lamellipodial actin networks in the P domain (Fig. 1e–h). Treatment with 5 μM VAS2870 reduced retrograde actin flow rates by 35% compared to DMSO pre-treatment (Fig. 1i; mean flow rates ± SEM were 4.6 ± 0.1 μm/min in DMSO vs. 3.0 ± 0.1 μm/min in VAS2870). Flow rates nearly recovered to control values following drug washout. Total neurite length per neuron was strongly reduced in neurons treated with 2.5 μM VAS2870 for a 24 h when compared to medium only or DMSO control conditions (Fig. 1j; 81% reduction compared to DMSO). Extensive drug washout over the following 24-h period did not reverse neurite length values. This is likely because of the significantly longer incubation time when compared to the results of the 20-min VAS2870 treatments. Using a different NADPH oxidase inhibitor, celastrol (Jaquet *et al.* 2011), we observed similar effects on growth cone morphology, actin flow, and neurite outgrowth (Figure S1). In summary, we found that treatment of cultured *Aplysia* neurons with VAS2870 or celastrol resulted in similar effects as our previous approaches of NADPH oxidase inhibition (Munnamalai and Suter 2009), confirming our findings that NADPH oxidase activity is critical for controlling actin organization and dynamics in growth cones as well as neurite growth.

Localization of a functional NOX2-type NADPH oxidase in neuronal growth cones

Although NOX1, NOX2, and NOX4 NADPH oxidase have been previously detected in cultured cerebellar granule neurons (Coyoy *et al.* 2008) and NOX2 additionally in hippocampal neurons (Tejada-Simon *et al.* 2005; Park and Jin 2008), sympathetic neurons (Tammariello *et al.* 2000; Hilburger *et al.* 2005), and dorsal root ganglion neurons (Cao *et al.* 2009), none of these studies investigated the localization of these enzyme complexes specifically in growth cones. Here, we identified a NOX2-type NADPH oxidase complex in growth cones using antibodies raised against human homologs of the membrane-bound NOX2 (Quinn *et al.* 1989) and cytosolic $p40^{phox}$ subunits (Gauss

et al. 2002). Western blotting of *Aplysia* CNS protein extracts with these antibodies detected a major band at the expected molecular weights of 75 kDa and 40 kDa, respectively (Fig. 2a). NOX2 proteins run as broad band between 73 and 91 kDa on SDS-PAGE, and the band pattern depends on the species and glycosylation (Quinn *et al.* 1989; Gauss *et al.* 2002; Krijnen *et al.* 2003).

Immunolabeling of cultured *Aplysia* bag cell neurons with these NOX2 and $p40^{phox}$ antibodies revealed a punctate pattern of both proteins within growth cones (Fig. 2b–c). NOX2 labeling in the P domain is more uniform and dense than $p40^{phox}$ labeling, which is expected for a plasma membrane-associated protein. NOX2 signals were markedly higher in the C domain of the growth cone (Fig. 2b) compared to the P domain, which can be attributed to NOX2's association with vesicles. Pre-incubation of the rabbit anti-NOX2 antibody with either the human peptide used for raising the antibody or the corresponding *Aplysia* peptide significantly reduced the fluorescence intensity in the growth cone periphery (Figure S2), providing evidence for the specificity of the NOX2 immunolabeling. Double labeling of NOX2 and the cell adhesion molecule apCAM revealed a partial colocalization between the two membrane-bound proteins. While apCAM was homogenous across the growth cone, NOX2 was more concentrated in discrete puncta (Figure S3). Further evidence for plasma membrane association of NOX2 in unstimulated *Aplysia* neurons is given by confocal imaging of the large neuronal cell body (Figure S4). The localization of the cytosolic $p40^{phox}$ subunit differed from NOX2 in a few ways. First, $p40^{phox}$ exhibited a striking array-like localization (Fig. 2c), very similar to F-actin bundles in the P domain. Second, the labeling in the C domain was not increased as in the case of NOX2. Third, hardly any $p40^{phox}$ was found in very thin growth cone regions that were clearly NOX2 positive (arrowhead in Fig. 2c and 3c).

NADPH oxidase produces superoxide, which can be converted quickly into H_2O_2, a ROS that has a longer half-life than superoxide and is likely involved in many ROS-mediated signaling processes (Bedard and Krause 2007; Winterbourn 2008). We used Peroxyfluor-6 acetoxymethyl ester (PF-6) as a H_2O_2-specific fluorescent dye (Dickinson *et al.* 2011) in combination with Calcein Red-Orange AM as a volume marker to perform ratiometric quantification of H_2O_2 levels in the growth cone P domain following activation and inhibition of NADPH oxidase (Fig. 2d–i). PF-6 signals were the highest in the C domain, specifically in mitochondria, a well-known ROS source, as well as in T zone ruffles. NADPH oxidase inhibition with 5 μM VAS2870 reduced H_2O_2 levels more than the DMSO control treatment after 15 min (Fig. 2d–h; 30% reduction by VAS2870; 16% reduction by DMSO), although these reductions were not significantly different (Student's *t*-test; $p = 0.12$). Conversely, we used the phorbol ester phorbol 12,13-dibutyrate (PDBu) to activate PKC, which is known to stimulate activity of NADPH oxidase through phosphorylation of p47phox (Fontayne *et al.* 2002). Within 30 s of PDBu application, H_2O_2 levels increased by 12 ± 3%. This PDBu-induced rise in H_2O_2 levels could be significantly decreased by coincubation with 5 μM VAS2870 to levels that were similar to basal H_2O_2 levels (Fig. 2i). In summary, immunolocalization and ROS imaging data further confirmed the presence of a functional NADPH oxidase complex in neuronal growth cones.

$p40^{phox}$ localization is F-actin dependent

Since $p40^{phox}$ exhibited an F-actin-like distribution, we performed triple labeling with phalloidin, $p40^{phox}$, and NOX2 antibodies to determine a potential colocalization between $p40^{phox}$ and F-actin (Fig. 3). In the growth cone P domain, $p40^{phox}$ exhibited only a partial overlap with NOX2 (Fig. 3e; inset e'). 38 ± 2% of $p40^{phox}$ colocalized with NOX2, while 22 ± 1% of NOX2 overlapped with $p40^{phox}$ (Fig. 3g). The highest colocalization between $p40^{phox}$ and NOX2 was found in the neck of the growth cone, which consolidates into the axon, as well as in contact areas between two adjacent growth cones (arrow in Fig. 3e). Little colocalization between $p40^{phox}$ and NOX2 was detected at the plasma membrane of neuronal cell bodies, while we found punctate structures inside the cell body that were labeled with both antibodies (Figure S4). On the other hand, $p40^{phox}$ exhibited higher colocalization with filopodial F-actin bundles in the growth cone periphery (Fig. 3f; inset f'), when compared to NOX2-colocalization with F-actin (Fig. 3g; 56 ± 3% vs. 47 ± 2%; $*p < 0.05$).

To further investigate the relationship between $p40^{phox}$, NOX2, and F-actin, we analyzed their distribution in growth cones with different amounts of F-actin. Most growth cones exhibit a typical actin organization with filopodial actin bundles in the P domain (growth cone in lower left of Fig. 4). These growth cones were rich in $p40^{phox}$ in the P domain. A smaller fraction of flat growth cones that are devoid of F-actin had very little $p40^{phox}$ in the P domain (growth cone in upper right of Fig. 4). These growth cones only exhibited $p40^{phox}$ signals in areas where the microtubule- and organelle-rich C domain invades the F-actin-free P domain. On the other hand, NOX2 signals in the P domain did not vary that much between growth cones containing different amounts of F-actin (Fig. 4c).

To confirm this correlation between $p40^{phox}$ and the F-actin localization, growth cones were treated with two different concentrations of cytochalasin B to perturb the F-actin organization (Fig. 5). A low dose of cytochalasin B (350 nM) resulted in the disruption of F-actin bundles but preservation of the F-actin meshwork (Burnette *et al.* 2008). Along with the disruption of F-actin bundles, we observed a 32% decrease in $p40^{phox}$ levels within the P domain (Fig. 5j; ANOVA, $**p < 0.01$). A high dose of cytochalasin B (5 μM)

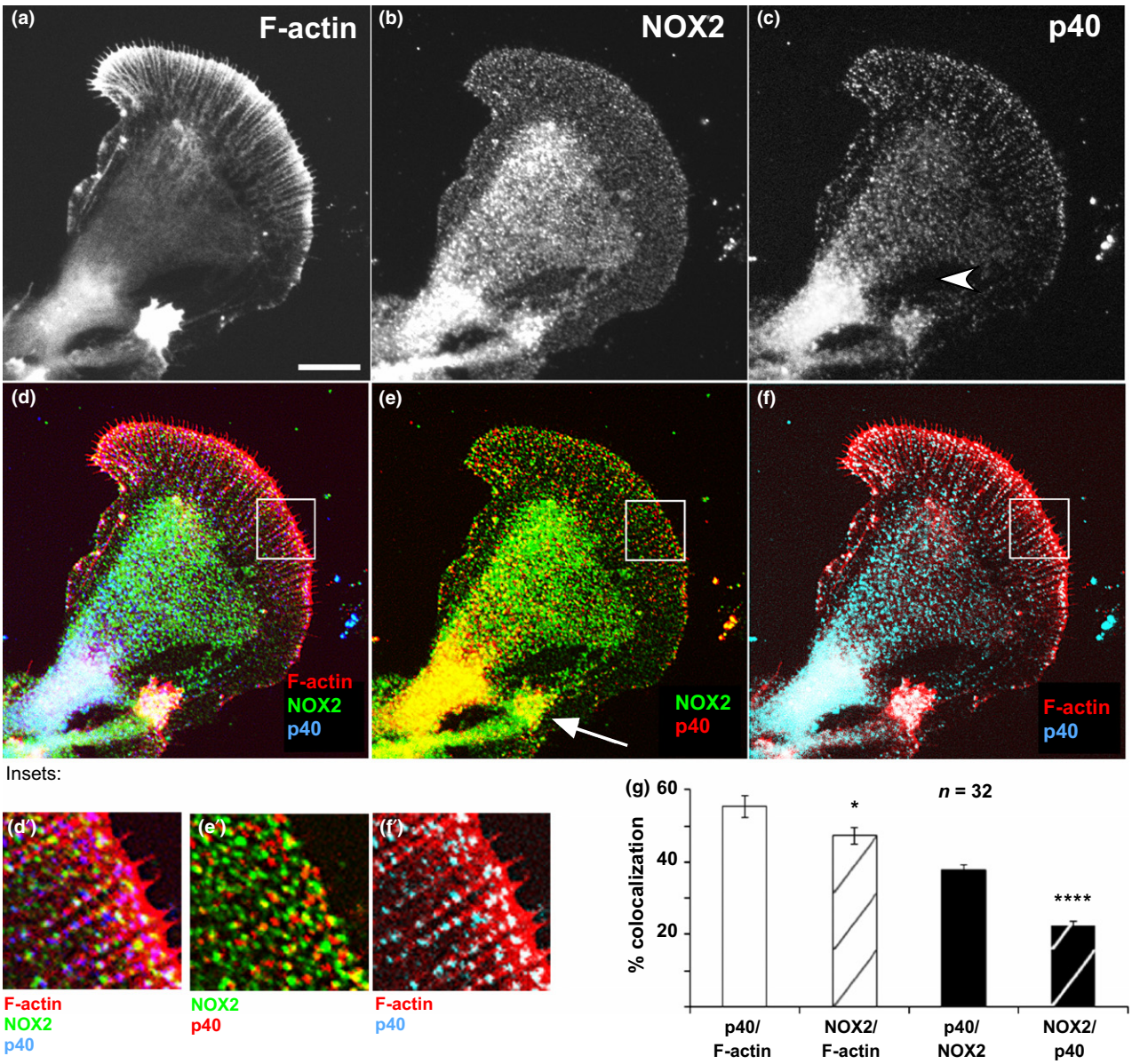

Fig. 3 p40^{phox} colocalizes with F-actin bundles. (a) *Aplysia* growth cone labeled for F-actin using Alexa 488-phalloidin. (b) NOX2 localization is strongest in the C domain and axon shaft. (c) p40^{phox} labeling exhibits an array-like pattern along F-actin bundles. No labeling in very flat area indicated by arrowhead. (d) Overlay of all three labels (red: F-actin; green: NOX2; blue: p40^{phox}) shows highest overlap in areas of growth cone–growth cone contact (bottom). (d') 3x enlarged inset of the boxed region of interest in the P domain shown in (d). (e) Overlay of NOX2 (green) and p40^{phox} (red). There is relatively little overlap of NOX2 and p40^{phox} in the growth cone periphery but more colocalization in the axon shaft and at growth cone–growth cone contacts (arrow). (e') Inset shows enlarged region of interest. (f) Overlay of F-actin (red) and p40^{phox} (blue) revealing colocalization of p40^{phox} and F-actin along filopodial bundles. (f') Inset shows enlarged region of interest. (g) Quantification of colocalization in growth cone P domain. NOX2 exhibits less colocalization with F-actin than p40^{phox} with F-actin (Student's *t*-test, $*p < 0.05$; $n = 32$ growth cones). The percentage of NOX2 colocalizing with p40^{phox} is lower than the percentage of p40^{phox} colocalizing with NOX2 (Student's *t*-test, $****p < 0.0001$). Scale bar: 10 μm.

strongly inhibited F-actin assembly in bundles and meshwork in the P domain. As retrograde actin flow continued, this treatment resulted in clearing of all F-actin structures from of the P domain besides a cytochalasin-resistant band of F-actin at the leading edge (Forscher and Smith 1988). p40^{phox} localization was completely disrupted in the region of actin clearance, and its levels decreased by 74% (Fig. 5i–j; $****p < 0.0001$). Interestingly, NOX2 levels were also reduced by cytochalasin B treatment (17% by 350 nM cytochalasin B, ANOVA, $**p < 0.01$; 58% by 5 μM

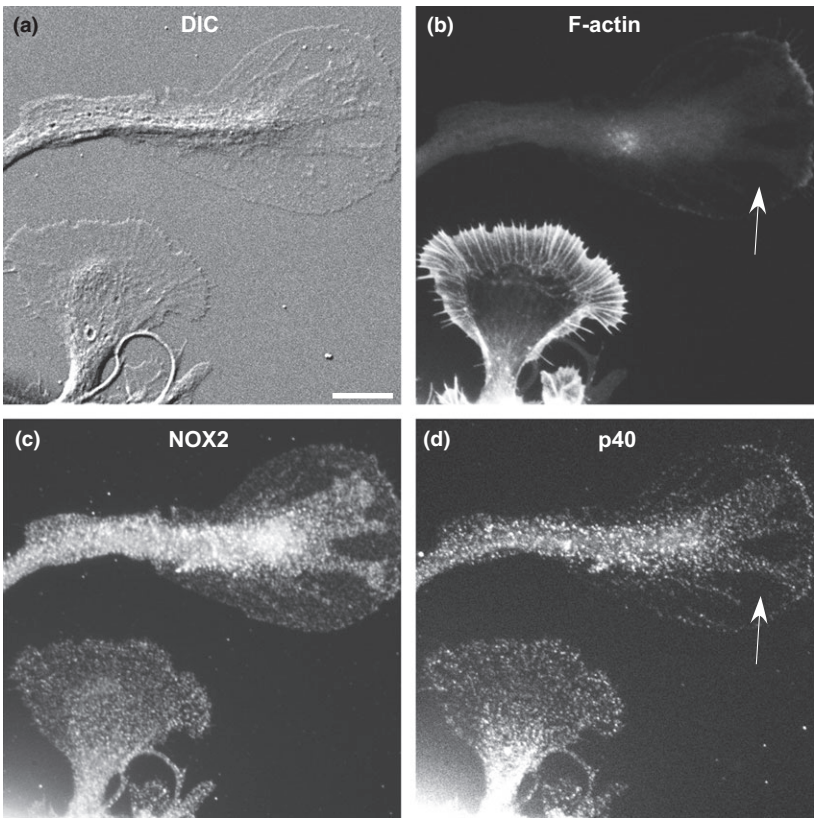

Fig. 4 p40^{phox} levels in the growth cone periphery correlate with F-actin content. (a) Differential interference contrast (DIC) image of two adjacent growth cones. The upper growth cone has a flat P domain with C domain expanding into the periphery. The lower growth cone exhibits a more typical morphology. (b) The upper growth cone above has significantly less F-actin when compared with the lower growth cone. (c) The upper growth cone exhibits NOX2 localized at the plasma membrane in the P domain. The NOX2-rich C domain has extended toward the leading edge of the growth cone, possibly because of the reduced amount of F-actin. The lower growth cone shows a typical homogenous NOX2 distribution. (d) The upper growth cone with little F-actin contains p40^{phox} only in areas where the C domain extended but not in flat regions (arrow). The lower growth cone with typical F-actin content contains higher levels of p40^{phox} than the upper one. Scale bar: 10 μm.

cytochalasin B, ****$p < 0.0001$). In summary, our results suggest that the growth cone localization of p40^{phox}, as well as of NOX2, depends on F-actin.

F-actin association of p40^{phox}

To further demonstrate a potential association of p40^{phox} with the F-actin cytoskeleton, we performed subcellular fractionation of *Aplysia* CNS tissue lysates (Fig. 6a). As expected, NOX2 was enriched in the plasma membrane compared to the cytoskeletal fraction and was not removed from this fraction following DNase 1 treatment, which reduces membrane-associated F-actin (Fig. 6a). On the other hand, p40^{phox} was more prominent in cytoskeletal than in membrane fractions. The distribution of p40^{phox} in the various cytoskeletal fractions (cytoskeletal, cytochalasin B-sensitive cytoskeletal, cytochalasin B-resistant cytoskeletal) showed a similar pattern as actin, indicating that a significant portion of p40^{phox} fractionates together with F-actin. The ratio of cytoskeletal over membrane-associated protein was higher for p40^{phox} when compared to NOX2 (Fig. 6b; 1.08 ± 0.05 for p40^{phox} vs. 0.76 ± 0.03 for NOX2; paired Student's *t*-test, $p = 0.05$). In addition, we detected p40^{phox} in actin immunoprecipitations from *Aplysia* CNS lysates (Fig. 6c). In summary, immunolocalization and biochemical data strongly suggest that the cytosolic subunit p40^{phox} associates with the F-actin cytoskeleton in unstimulated neurons, while localization of the membrane subunit NOX2 appears less dependent on F-actin.

Enhanced p40^{phox}–NOX2 colocalization in apCAM-evoked growth

To investigate whether p40^{phox} and NOX2 distribution changes following growth cone stimulation with adhesive cues, we performed the restrained bead interaction (RBI) assay utilizing beads coated with the *Aplysia* cell adhesion molecule apCAM (Suter *et al.* 1998, 2004). Since considerable actin remodeling occurs around beads during apCAM-evoked growth, we tested whether NOX2 and p40^{phox} localization was altered during these events. We found a significant increase of both p40^{phox} and NOX2 signals in vicinity of apCAM beads when compared to adjacent non-RBI areas (Fig. 7a–d). Furthermore, there was a significantly higher colocalization of p40^{phox} and NOX2 when compared with non-RBI areas (Fig. 7d–e; 71.4 ± 4.0% colocalization in bead areas vs. 29.5 ± 4.8% in non-RBI areas; $n = 4$ RBI experiments; Student's *t*-test: ***$p < 0.001$). In the example shown here, the staining for NOX2 and p40^{phox} appeared reduced in the C domain that extended toward the restrained bead when compared to C domain labeling of control growth cones. However, we did not observe this reduction consistently in other experiments. These findings indicate that apCAM-mediated adhesion could result in NOX2 cytosolic

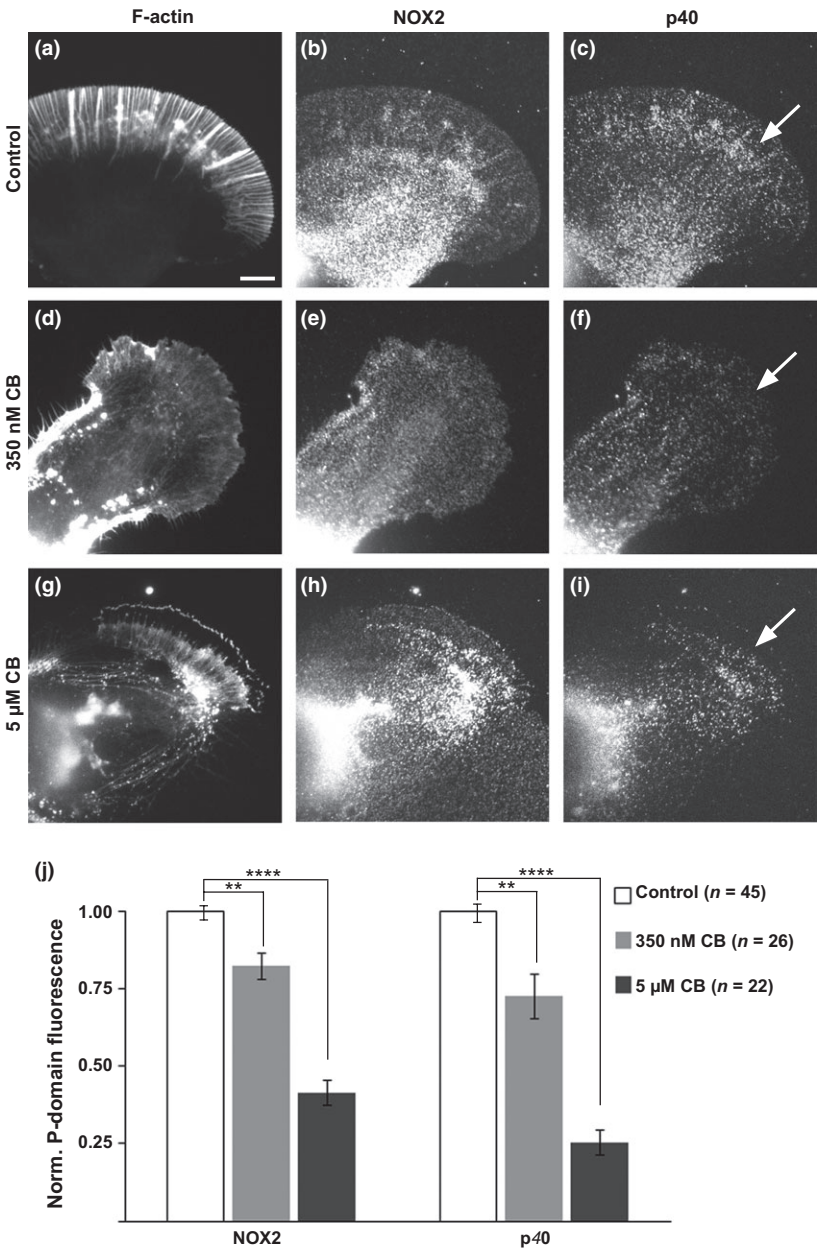

Fig. 5 Cytochalasin B perturbs p40^{phox} and NOX2 localization (a–c) F-actin, NOX2, and p40^{phox} labeling of a control growth cone. (d–f) F-actin, NOX2, and p40^{phox} labeling in a growth cone treated with 350 nM cytochalasin B to diminish F-actin bundles. NOX2 localization appears typical of control growth cones, while the distinctive bundle-like localization of p40^{phox} is abolished by 350 nM cytochalasin B treatment. (g–i) F-actin, NOX2 and p40^{phox} labeling in a growth cone treated with 5 µM cytochalasin B. Both p40^{phox} and NOX2 signals are reduced in the F-actin-free region. (j) Quantification of the NOX2 and p40^{phox} levels in the P domain. Average values ± SEM of background-subtracted fluorescence intensities are shown after normalization to controls (ANOVA; $^{**}p < 0.01$; $^{****}p < 0.0001$; n = growth cones from three independent experiments). Scale bars: 10 µm.

subunit recruitment and potential NADPH oxidase activation that involves F-actin remodeling.

Discussion

This is the first report on subcellular localization of NADPH oxidase in neuronal growth cones. Expression of NOX1-NOX4 family members at the RNA and protein levels has been shown for various brain regions including cortex, cerebellum, hippocampus, as well as for peripheral ganglia (Sorce and Krause 2009; Hernandes and Britto 2012). NOX2 subunits have been localized in cultured neurons, such as hippocampal (Tejada-Simon *et al.* 2005; Park and Jin 2008), cerebellar granule (Coyoy *et al.* 2008), sympathetic (Tammariello *et al.* 2000; Hilburger *et al.* 2005), and dorsal root ganglion neurons (Cao *et al.* 2009). However, these studies did not investigate the detailed subcellular distribution of NADPH oxidase proteins. Here, we have shown that a NOX2-type NADPH oxidase is localized to the plasma membrane of *Aplysia* neuronal growth cones, exhibiting a similar but less homogenous plasma membrane distribution compared to the cell adhesion protein apCAM. Whether another type of NADPH oxidase is also present in *Aplysia* growth cones, remains to be investigated. NADPH oxidase inhibition with VAS2870 or celastrol impaired actin organization and dynamics as well as neurite outgrowth, confirming

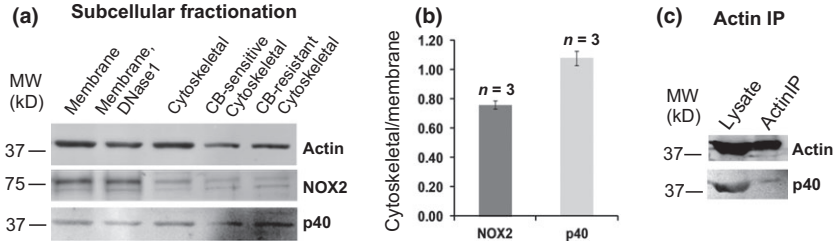

Fig. 6 Biochemical evidence for actin association of p40^{phox}. (a) Subcellular fractionation revealed that p40^{phox} is more predominant in cytoskeletal fractions while NOX2 is more prominent in membrane fractions. (b) Quantification of immunoblots showed that the ratio of cytoskeletal/membrane protein is higher for p40^{phox} than for NOX2. (c) p40^{phox} coimmunoprecipates with actin from *Aplysia* CNS lysates.

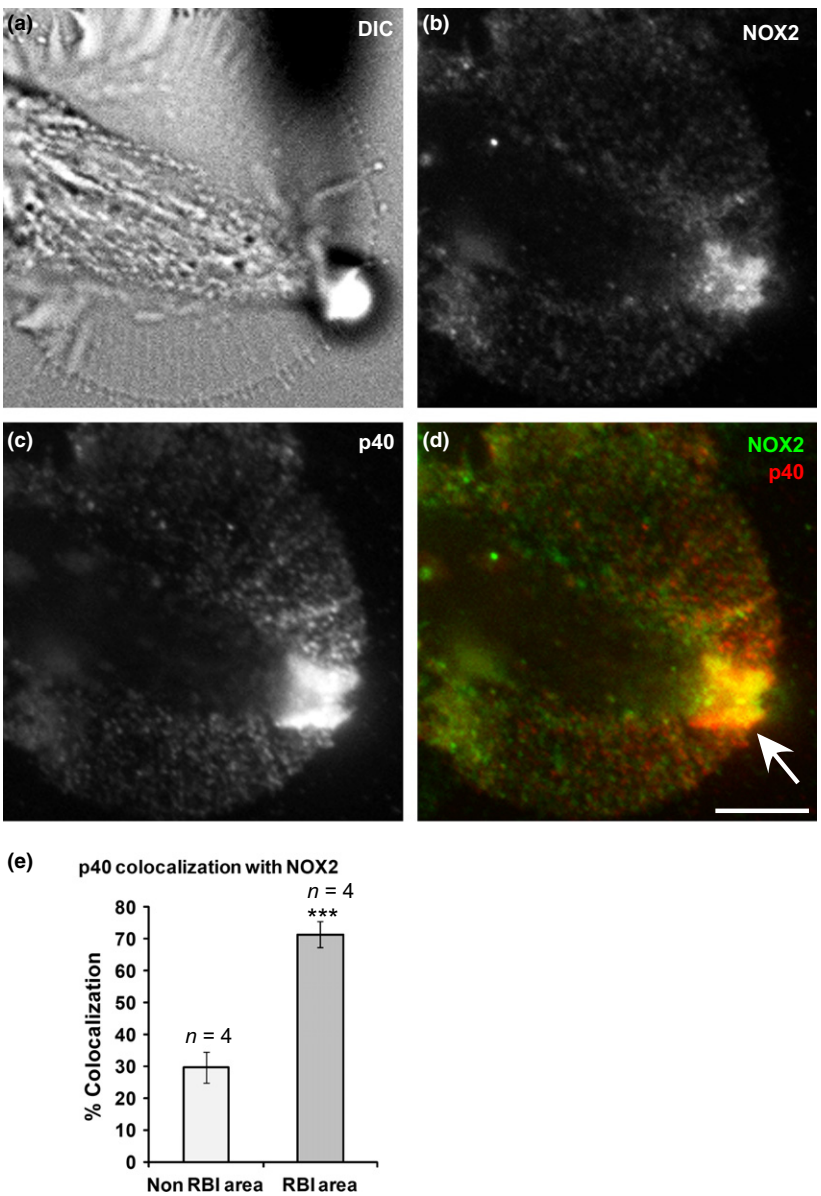

Fig. 7 Increased colocalization of p40^{phox} with NOX2 at apCAM adhesion sites. (a) differential interference contrast (DIC) image of growth cone after completion of restrained bead interaction with apCAM bead. The C domain has extended toward the bead. (b) Increased NOX2 signals around apCAM beads after completed interactions. (c) p40^{phox} levels are also highly increased at adhesion site. (d) Overlay shows increased colocalization of p40^{phox} and NOX2 near adhesion site (arrow) compared to adjacent areas in the growth cone periphery. Scale bar: 10 μm. (e) Quantification of p40^{phox}/NOX2 colocalization. Colocalization was quantified by determining the percentage of area overlap between the two signals.

our previous findings (this study; Munnamalai and Suter 2009), while NADPH oxidase activation increased H_2O_2 levels in the growth cone P domain (Figs. 1–2; Figure S1). The cytosolic subunit $p40^{phox}$ exhibited relatively little colocalization with NOX2 in unstimulated growth cones, but had significant colocalization with F-actin bundles (Fig. 3). We observed variations in $p40^{phox}$ levels between growth cones, which correlated with F-actin content (Fig. 4). Cytochalasin B significantly reduced the amount of $p40^{phox}$ in the growth cone periphery (Fig. 5), while cell fractionation and actin coimmunoprecipitation experiments confirmed a partial association of $p40^{phox}$ with F-actin (Fig. 6). Cell fractionation studies were performed on total CNS lysates suggesting that the differential association of NOX2 and $p40^{phox}$ not only occurs in the growth cone but also in other regions of the cell. Differential localization of NOX2 and $p40^{phox}$ in other compartments of unstimulated neurons is further supported by confocal imaging of the neuronal cell body (Figure S4). Finally, we have found increased $p40^{phox}$/NOX2 colocalization at adhesion sites during apCAM-evoked neuronal growth (Fig. 7). In summary, these findings provide evidence for a bidirectional functional relationship between NADPH oxidase activity and the actin cytoskeleton in neuronal growth cones, which may contribute to the control of neurite outgrowth.

Very little is known about NADPH oxidase signaling in neuronal development, particularly in axonal growth and guidance. Previous work from our laboratory and others suggested a role for NADPH oxidase-derived ROS in regulating neurite outgrowth (Suzukawa *et al.* 2000; Ibi *et al.* 2006; Munnamalai and Suter 2009). Tail wound-derived H_2O_2 can promote regeneration of sensory axons in Zebrafish embryos (Rieger and Sagasti 2011). Furthermore, we have shown that NADPH oxidase inhibition in *Aplysia* growth cones results in reduced F-actin content (this study; Munnamalai and Suter 2009). ROS have also been implicated in Rac1-dependent Ca^{2+} release in *Aplysia* growth cones (Zhang and Forscher 2009). Because of the short half-life and high reactivity of ROS, target proteins need to be close to the ROS source to establish signaling specificity (Ushio-Fukai 2006). Consistent with this idea, we found NADPH oxidase localized in the growth cone periphery at sites where actin assembly occurs. This study is also interesting from an evolutionary point of view. While ancestral NOX2, $p22^{phox}$, $p47^{phox}$, and $p67^{phox}$ homologs have been identified for several invertebrate species including *Monosiga brevicollis, Nematostella vectensis, Strongylocentrotus purpuratus,* as well as the snail *Lottia gigantea*, no $p40^{phox}$ homolog has been identified in these species thus far, which has led to the conclusion that $p40^{phox}$ may have evolved later with the chordata (Kawahara *et al.* 2007; Sumimoto 2008). Very recently several predicted *Aplysia* NADPH oxidase-like sequences have been released to the NCBI database, including NOX2-like (XP_005090645), NOX5-like XP_005101964), dual oxidase 1 (DUOX1)-like (XP_005108327), and DUOX2-like (XP_005106629). Our results suggest that a NOX2-type NADPH complex with all membrane and cytosolic subunits including the regulatory subunit $p40^{phox}$ already evolved with the appearance of the molluscan clade. Other available antibodies against NOX2-type subunits did not detect proteins with high enough specificity (data not shown); thus, because of this limitation we were unable to detect other subunits of the NOX2-type complex in *Aplysia* growth cones thus far.

Our quantification of H_2O_2 levels following PKC activation revealed that the NADPH oxidase is functionally active in growth cones. VAS2870 abolished the PDBu-stimulated increase in H_2O_2 levels in the growth cone periphery within 30 s (Fig. 2i). Treatment of growth cones with VAS2870 alone for 15 min resulted only in a modest decrease of H_2O_2 levels (Fig. 2h). These findings are in line with another study demonstrating that VAS2870 blocked the increase of ROS levels in endothelial cells activated by oxidized low-density lipoprotein, but had minimal effect on the basal ROS levels without stimulation (Stielow *et al.* 2006). There are several possible reasons why VAS2870 treatment alone did not lower basal H_2O_2 levels more. First, NADPH oxidases are not the only source for superoxide/hydrogen peroxide. Second, we are measuring hydrogen peroxide in this assay and not superoxide, which is the primary product of NADPH oxidase. Third, ROS are highly reactive, act locally, and are tightly regulated. Finally, the dye used to detect hydrogen peroxide may not be able to detect small ROS changes. Thus, it might be difficult to optically detect local changes in ROS levels induced by NADPH oxidase inhibition with sufficient temporal resolution, despite the fact that such changes can affect cellular physiology and morphology.

Cytoskeletal association of regulatory NOX subunits has been reported for $p40^{phox}$, $p47^{phox}$, and $p67^{phox}$ in non-neuronal cells (Nauseef *et al.* 1991; El Benna *et al.* 1994, 1999; Li and Shah 2002). Furthermore, $p40^{phox}$ and $p47^{phox}$ associate with the neutrophil cytoskeleton through a PX-domain-dependent interaction with the actin-associated protein moesin (Wientjes *et al.* 2001; Zhan *et al.* 2004), while $p40^{phox}$ also interacts with the actin-binding protein coronin (Grogan *et al.* 1997), as well as directly with the actin cytoskeleton (Shao *et al.* 2010). These findings suggested that actin association of cytosolic NADPH oxidase subunits may have a regulatory function by keeping the complex in an inactive state until a stimulus releases the subunits from the cytoskeleton during the activation process. In agreement with this idea, COS-7 expression experiments revealed that $p40^{phox}$ is associated with actin and moesin, and that a mutated form of $p40^{phox}$ shows higher actin association and inhibits NOX2 activity (Chen *et al.* 2007). Furthermore, the actin-binding protein cortactin has been suggested to regulate NOX2 activation in lung endothelial cells trough an interaction with $p47^{phox}$ (Usatyuk *et al.* 2007). Thus, actin rearrangements could also deliver cytosolic NADPH oxidase

subunits to the plasma membrane. Does NOX2 localization show actin dependence? In migrating endothelial cells, NOX2 colocalizes with F-actin along the leading edge in an IQ motif containing GTPase activating protein 1 (IQGAP1)-dependent manner, while manipulating the actin cytoskeleton with latrunculin and jasplakinolide alters NOX2 localization (Ikeda *et al.* 2005). Our growth cone studies also suggest a certain actin dependence of NOX2 localization as indicated by the reduction of NOX2 following cytochalasin treatment and the colocalization of NOX2 with actin along the leading edge and in transition zone ruffle/intrapodia (Fig. 5g and h). Thus, a fraction of NOX2 along with $p40^{phox}$ appears to undergo retrograde flow together with F-actin. In summary, our present work in neuronal growth cones is consistent with previous findings made with leukocytes and endothelial cells indicating that the actin cytoskeleton may play a role in NADPH oxidase activation through localization of its subunits.

On the other hand, NADPH oxidase-derived ROS regulate actin organization and dynamics, growth cone motility, and neurite growth (this study; Munnamalai and Suter 2009) and actin organization and migration of non-neuronal cells (Nimnual *et al.* 2003; Wojciak-Stothard *et al.* 2005; Schroder *et al.* 2007; Kim *et al.* 2009, 2011; Kuiper *et al.* 2011). Thus, together with these findings, our current study suggests an interesting bidirectional relationship between NADPH oxidase and F-actin. We propose that the cytosolic NADPH oxidase subunits such as p40 are associated with actin structures in unstimulated growth cones. Upon growth cone stimulation by guidance cues, cytosolic subunits $p47^{phox}$, $p67^{phox}$, $p40^{phox}$, and Rac1 translocate to the plasma membrane (either with or without F-actin) and activate the membrane-bound subunits NOX2/$p22^{phox}$. NADPH oxidase-produced superoxide (or most likely hydrogen peroxide) diffuses back into the growth cone for local regulation of the cytoskeleton and related directional growth (see graphical abstract of the online version). In agreement with this hypothesis, we found increased $p40^{phox}$/NOX2 levels and colocalization at growth cone contact sites with apCAM beads (Fig. 7) and interacting growth cones (arrow in Fig. 3e), where apCAM exhibits increased density as well (Thompson *et al.* 1996; Suter *et al.* 1998). These results indicate that apCAM clustering can trigger actin remodeling as well as NADPH oxidase activation related to neurite outgrowth. The details of the functional relationship and order of events of apCAM clustering, actin reorganization, and NADPH oxidase activation remain unclear at this point. apCAM clustering could first activate NADPH oxidase followed by ROS-mediated actin reorganization; or apCAM-mediated actin remodeling could activate NOX2 by translocating cytosolic subunits close to plasma membrane. Thus, additional studies are needed to address the important question whether NADPH oxidase activation plays a functional role in axonal growth triggered by apCAM or other guidance cues.

Acknowledgements and conflict of interests disclosure

We thank members of the Suter laboratory for their comments on this manuscript. PF-6 AM was kindly provided to us by Dr. Christopher Chang and Vivian Lin, University of California, Berkeley CA, USA. We also thank Kelsey Martin, Samuel Schacher, and Eric Kandel for providing 4E8 hybridoma cells to produce 4E8 antibody. This work was supported by grants from the NIH (R01 NS049233 to D.M.S. and P20 GM103500 to M. Q.), NSF (1146944-IOS to D.M.S.), and the Bindley Bioscience Center at Purdue University (D.M.S.). V. M. was partially supported by fellowships through the PULSe and PUN Integrative Neuroscience graduate programs at Purdue University. The authors have no conflict of interest to declare.

All experiments were conducted in compliance with the ARRIVE guidelines. The authors have no conflict of interest to declare.

Supporting information

Additional supporting information may be found in the online version of this article at the publisher's web-site:

Figure S1. NADPH oxidase inhibition via celastrol reduces retrograde flow and neurite outgrowth.

Figure S2. Peptide blocking control experiment for NOX2 immunolabeling.

Figure S3. NOX2 partially colocalizes with apCAM in the plasma membrane.

Figure S4. Distinct subcellular localizations NOX2 and p40phox in the cell body.

Video S1. VAS2870 effects on growth cone morphology and motility.

References

Altenhofer S., Kleikers P. W., Radermacher K. A., Scheurer P., Rob Hermans J. J., Schiffers P., Ho H., Wingler K. and Schmidt H. H. (2012) The NOX toolbox: validating the role of NADPH oxidases in physiology and disease. *Cell. Mol. Life Sci.* **69**, 2327–2343.

Barth B. M., Gustafson S. J. and Kuhn T. B. (2012) Neutral sphingomyelinase activation precedes NADPH oxidase-dependent damage in neurons exposed to the proinflammatory cytokine tumor necrosis factor-alpha. *J. Neurosci. Res.* **90**, 229–242.

Bedard K. and Krause K. H. (2007) The NOX family of ROS-generating NADPH oxidases: physiology and pathophysiology. *Physiol. Rev.* **87**, 245–313.

Brennan A. M., Suh S. W., Won S. J., Narasimhan P., Kauppinen T. M., Lee H., Edling Y., Chan P. H. and Swanson R. A. (2009) NADPH oxidase is the primary source of superoxide induced by NMDA receptor activation. *Nat. Neurosci.* **12**, 857–863.

Burnette D. T., Ji L., Schaefer A. W., Medeiros N. A., Danuser G. and Forscher P. (2008) Myosin II activity facilitates microtubule bundling in the neuronal growth cone neck. *Dev. Cell* **15**, 163–169.

Camello-Almaraz M. C., Pozo M. J., Murphy M. P. and Camello P. J. (2006) Mitochondrial production of oxidants is necessary for physiological calcium oscillations. *J. Cell. Physiol.* **206**, 487–494.

Cao X., Demel S. L., Quinn M. T., Galligan J. J. and Kreulen D. (2009) Localization of NADPH oxidase in sympathetic and sensory ganglion neurons and perivascular nerve fibers. *Auton. Neurosci.* **151**, 90–97.

Chen J., He R., Minshall R. D., Dinauer M. C. and Ye R. D. (2007) Characterization of a mutation in the Phox homology domain of the NADPH oxidase component p40phox identifies a mechanism for negative regulation of superoxide production. *J. Biol. Chem.* **282**, 30273–30284.

Chiarugi P., Pani G., Giannoni E. *et al.* (2003) Reactive oxygen species as essential mediators of cell adhesion: the oxidative inhibition of a FAK tyrosine phosphatase is required for cell adhesion. *J. Cell Biol.* **161**, 933–944.

Coyoy A., Valencia A., Guemez-Gamboa A. and Moran J. (2008) Role of NADPH oxidase in the apoptotic death of cultured cerebellar granule neurons. *Free Radic. Biol. Med.* **45**, 1056–1064.

Dickinson B. C., Peltier J., Stone D., Schaffer D. V. and Chang C. J. (2011) Nox2 redox signaling maintains essential cell populations in the brain. *Nat. Chem. Biol.* **7**, 106–112.

El Benna J., Ruedi J. M. and Babior B. M. (1994) Cytosolic guanine nucleotide-binding protein Rac2 operates in vivo as a component of the neutrophil respiratory burst oxidase. Transfer of Rac2 and the cytosolic oxidase components p47phox and p67phox to the submembranous actin cytoskeleton during oxidase activation. *J. Biol. Chem.* **269**, 6729–6734.

El Benna J., Dang P. M., Andrieu V. *et al.* (1999) P40phox associates with the neutrophil Triton X-100-insoluble cytoskeletal fraction and PMA-activated membrane skeleton: a comparative study with P67phox and P47phox. *J. Leukoc. Biol.* **66**, 1014–1020.

Finkel T. (2011) Signal transduction by reactive oxygen species. *J. Cell Biol.* **194**, 7–15.

Fontayne A., Dang P. M., Gougerot-Pocidalo M. A. and El-Benna J. (2002) Phosphorylation of p47phox sites by PKC alpha, beta II, delta, and zeta: effect on binding to p22phox and on NADPH oxidase activation. *Biochemistry* **41**, 7743–7750.

Forscher P. and Smith S. J. (1988) Actions of cytochalasins on the organization of actin filaments and microtubules in a neuronal growth cone. *J. Cell Biol.* **107**, 1505–1516.

ten Freyhaus H., Huntgeburth M., Wingler K. *et al.* (2006) Novel Nox inhibitor VAS2870 attenuates PDGF-dependent smooth muscle cell chemotaxis, but not proliferation. *Cardiovasc. Res.* **71**, 331–341.

Gao H. M., Zhou H. and Hong J. S. (2012) NADPH oxidases: novel therapeutic targets for neurodegenerative diseases. *Trends Pharmacol. Sci.* **33**, 295–303.

Gauss K. A., Mascolo P. L., Siemsen D. W., Nelson L. K., Bunger P. L., Pagano P. J. and Quinn M. T. (2002) Cloning and sequencing of rabbit leukocyte NADPH oxidase genes reveals a unique p67 (phox) homolog. *J. Leukoc. Biol.* **71**, 319–328.

Grogan A., Reeves E., Keep N., Wientjes F., Totty N. F., Burlingame A. L., Hsuan J. J. and Segal A. W. (1997) Cytosolic phox proteins interact with and regulate the assembly of coronin in neutrophils. *J. Cell Sci.* **110**(Pt 24), 3071–3081.

Guemez-Gamboa A. and Moran J. (2009) NOX2 mediates apoptotic death induced by staurosporine but not by potassium deprivation in cerebellar granule neurons. *J. Neurosci. Res.* **87**, 2531–2540.

Hernandes M. S. and Britto L. R. (2012) NADPH oxidase and neurodegeneration. *Curr. Neuropharmacol.* **10**, 321–327.

Heumuller S., Wind S., Barbosa-Sicard E., Schmidt H. H., Busse R., Schroder K. and Brandes R. P. (2008) Apocynin is not an inhibitor of vascular NADPH oxidases but an antioxidant. *Hypertension* **51**, 211–217.

Hilburger E. W., Conte E. J., McGee D. W. and Tammariello S. P. (2005) Localization of NADPH oxidase subunits in neonatal sympathetic neurons. *Neurosci. Lett.* **377**, 16–19.

Ibi M., Katsuyama M., Fan C., Iwata K., Nishinaka T., Yokoyama T. and Yabe-Nishimura C. (2006) NOX1/NADPH oxidase negatively regulates nerve growth factor-induced neurite outgrowth. *Free Radic. Biol. Med.* **40**, 1785–1795.

Ikeda S., Yamaoka-Tojo M., Hilenski L., Patrushev N. A., Anwar G. M., Quinn M. T. and Ushio-Fukai M. (2005) IQGAP1 regulates reactive oxygen species-dependent endothelial cell migration through interacting with Nox2. *Arterioscler. Thromb. Vasc. Biol.* **25**, 2295–2300.

Jaquet V., Scapozza L., Clark R. A., Krause K. H. and Lambeth J. D. (2009) Small-molecule NOX inhibitors: ROS-generating NADPH oxidases as therapeutic targets. *Antioxid. Redox Signal.* **11**, 2535–2552.

Jaquet V., Marcoux J., Forest E. *et al.* (2011) NADPH oxidase (NOX) isoforms are inhibited by celastrol with a dual mode of action. *Br. J. Pharmacol.* **164**, 507–520.

Kawahara B. T., Quinn M. T. and Lambeth J. D. (2007) Molecular evolution of the reactive oxygen-generating NADPH oxidase (Nox/Duox) family of enzymes. *BMC Evol. Biol.* **7**, 109.

Kim J. S., Huang T. Y. and Bokoch G. M. (2009) Reactive oxygen species regulate a slingshot-cofilin activation pathway. *Mol. Biol. Cell* **20**, 2650–2660.

Kim J. S., Bak E. J., Lee B. C., Kim Y. S., Park J. B. and Choi I. G. (2011) Neuregulin induces HaCaT keratinocyte migration via Rac1-mediated NADPH-oxidase activation. *J. Cell. Physiol.* **226**, 3014–3021.

Kishida K. T., Hoeffer C. A., Hu D., Pao M., Holland S. M. and Klann E. (2006) Synaptic plasticity deficits and mild memory impairments in mouse models of chronic granulomatous disease. *Mol. Cell. Biol.* **26**, 5908–5920.

Krijnen P. A., Meischl C., Hack C. E., Meijer C. J., Visser C. A., Roos D. and Niessen H. W. (2003) Increased Nox2 expression in human cardiomyocytes after acute myocardial infarction. *J. Clin. Pathol.* **56**, 194–199.

Kuiper J. W., Sun C., Magalhaes M. A. and Glogauer M. (2011) Rac regulates PtdInsP(3) signaling and the chemotactic compass through a redox-mediated feedback loop. *Blood* **118**, 6164–6171.

Le Cabec V. and Maridonneau-Parini I. (1995) Complete and reversible inhibition of NADPH oxidase in human neutrophils by phenylarsine oxide at a step distal to membrane translocation of the enzyme subunits. *J. Biol. Chem.* **270**, 2067–2073.

Lee A. C., Decourt B. and Suter D. (2008) Neuronal cell cultures from aplysia for high-resolution imaging of growth cones. *J. Vis. Exp.* **12**, 662.

Lee M. Y., San Martin A., Mehta P. K. *et al.* (2009) Mechanisms of vascular smooth muscle NADPH oxidase 1 (Nox1) contribution to injury-induced neointimal formation. *Arterioscler. Thromb. Vasc. Biol.* **29**, 480–487.

Li J. M. and Shah A. M. (2002) Intracellular localization and preassembly of the NADPH oxidase complex in cultured endothelial cells. *J. Biol. Chem.* **277**, 19952–19960.

Li L., Hutchins B. I. and Kalil K. (2009) Wnt5a induces simultaneous cortical axon outgrowth and repulsive axon guidance through distinct signaling mechanisms. *J. Neurosci.* **29**, 5873–5883.

Moldovan L., Moldovan N. I., Sohn R. H., Parikh S. A. and Goldschmidt-Clermont P. J. (2000) Redox changes of cultured endothelial cells and actin dynamics. *Circ. Res.* **86**, 549–557.

Munnamalai V. and Suter D. M. (2009) Reactive oxygen species regulate F-actin dynamics in neuronal growth cones and neurite outgrowth. *J. Neurochem.* **108**, 644–661.

Nauseef W. M., Volpp B. D., McCormick S., Leidal K. G. and Clark R. A. (1991) Assembly of the neutrophil respiratory burst oxidase. Protein kinase C promotes cytoskeletal and membrane association of cytosolic oxidase components. *J. Biol. Chem.* **266**, 5911–5917.

Nimnual A. S., Taylor L. J. and Bar-Sagi D. (2003) Redox-dependent downregulation of Rho by Rac. *Nat. Cell Biol.* **5**, 236–241.

Park K. W. and Jin B. K. (2008) Thrombin-induced oxidative stress contributes to the death of hippocampal neurons: role of neuronal NADPH oxidase. *J. Neurosci. Res.* **86**, 1053–1063.

Quinn M. T., Parkos C. A., Walker L., Orkin S. H., Dinauer M. C. and Jesaitis A. J. (1989) Association of a Ras-related protein with cytochrome b of human neutrophils. *Nature* **342**, 198–200.

Rieger S. and Sagasti A. (2011) Hydrogen peroxide promotes injury-induced peripheral sensory axon regeneration in the zebrafish skin. *PLoS Biol.* **9**, e1000621.

Schroder K., Helmcke I., Palfi K., Krause K. H., Busse R. and Brandes R. P. (2007) Nox1 mediates basic fibroblast growth factor-induced migration of vascular smooth muscle cells. *Arterioscler. Thromb. Vasc. Biol.* **27**, 1736–1743.

Shao D., Segal A. W. and Dekker L. V. (2010) Subcellular localisation of the p40phox component of NADPH oxidase involves direct interactions between the Phox homology domain and F-actin. *Int. J. Biochem. Cell Biol.* **42**, 1736–1743.

Sohal R. S. and Orr W. C. (2012) The redox stress hypothesis of aging. *Free Radic. Biol. Med.* **52**, 539–555.

Sorce S. and Krause K. H. (2009) NOX enzymes in the central nervous system: from signaling to disease. *Antioxid. Redox Signal.* **11**, 2481–2504.

Stielow C., Catar R. A., Muller G., Wingler K., Scheurer P., Schmidt H. H. and Morawietz H. (2006) Novel Nox inhibitor of oxLDL-induced reactive oxygen species formation in human endothelial cells. *Biochem. Biophys. Res. Commun.* **344**, 200–205.

Sumimoto H. (2008) Structure, regulation and evolution of Nox-family NADPH oxidases that produce reactive oxygen species. *FEBS J.* **275**, 3249–3277.

Suter D. M. (2011) Live cell imaging of neuronal growth cone motility and guidance in vitro. *Methods Mol. Biol.* **769**, 65–86.

Suter D. M., Errante L. D., Belotserkovsky V. and Forscher P. (1998) The Ig superfamily cell adhesion molecule, apCAM, mediates growth cone steering by substrate-cytoskeletal coupling. *J. Cell Biol.* **141**, 227–240.

Suter D. M., Schaefer A. W. and Forscher P. (2004) Microtubule dynamics are necessary for SRC family kinase-dependent growth cone steering. *Curr. Biol.* **14**, 1194–1199.

Suzukawa K., Miura K., Mitsushita J., Resau J., Hirose K., Crystal R. and Kamata T. (2000) Nerve growth factor-induced neuronal differentiation requires generation of Rac1-regulated reactive oxygen species. *J. Biol. Chem.* **275**, 13175–13178.

Taddei M. L., Parri M., Mello T., Catalano A., Levine A. D., Raugei G., Ramponi G. and Chiarugi P. (2007) Integrin-mediated cell adhesion and spreading engage different sources of reactive oxygen species. *Antioxid. Redox Signal.* **9**, 469–481.

Tammariello S. P., Quinn M. T. and Estus S. (2000) NADPH oxidase contributes directly to oxidative stress and apoptosis in nerve growth factor-deprived sympathetic neurons. *J. Neurosci.*, **20**, RC53.

Tejada-Simon M. V., Serrano F., Villasana L. E., Kanterewicz B. I., Wu G. Y., Quinn M. T. and Klann E. (2005) Synaptic localization of a functional NADPH oxidase in the mouse hippocampus. *Mol. Cell. Neurosci.* **29**, 97–106.

Thompson C., Lin C. H. and Forscher P. (1996) An Aplysia cell adhesion molecule associated with site-directed actin filament assembly in neuronal growth cones. *J. Cell Sci.* **109**(Pt 12), 2843–2854.

Usatyuk P. V., Romer L. H., He D. *et al.* (2007) Regulation of hyperoxia-induced NADPH oxidase activation in human lung endothelial cells by the actin cytoskeleton and cortactin. *J. Biol. Chem.* **282**, 23284–23295.

Ushio-Fukai M. (2006) Localizing NADPH oxidase-derived ROS. *Sci. STKE*, **2006**, re8.

Ushio-Fukai M., Tang Y., Fukai T. *et al.* (2002) Novel role of gp91 (phox)-containing NAD(P)H oxidase in vascular endothelial growth factor-induced signaling and angiogenesis. *Circ. Res.* **91**, 1160–1167.

Wientjes F. B., Reeves E. P., Soskic V., Furthmayr H. and Segal A. W. (2001) The NADPH oxidase components p47(phox) and p40 (phox) bind to moesin through their PX domain. *Biochem. Biophys. Res. Commun.* **289**, 382–388.

Wind S., Beuerlein K., Eucker T., Muller H., Scheurer P., Armitage M. E., Ho H., Schmidt H. H. and Wingler K. (2010) Comparative pharmacology of chemically distinct NADPH oxidase inhibitors. *Br. J. Pharmacol.* **161**, 885–898.

Winterbourn C. C. (2008) Reconciling the chemistry and biology of reactive oxygen species. *Nat. Chem. Biol.* **4**, 278–286.

Wojciak-Stothard B., Tsang L. Y. and Haworth S. G. (2005) Rac and Rho play opposing roles in the regulation of hypoxia/reoxygenation-induced permeability changes in pulmonary artery endothelial cells. *Am. J. Physiol. Lung Cell. Mol. Physiol.* **288**, L749–L760.

Yang Y., Karakhanova S., Werner J. and Bazhin A. V. (2013) Reactive oxygen species in cancer biology and anticancer therapy. *Curr. Med. Chem.* **20**, 3677–3692.

Zhan Y., He D., Newburger P. E. and Zhou G. W. (2004) p47(phox) PX domain of NADPH oxidase targets cell membrane via moesin-mediated association with the actin cytoskeleton. *J. Cell. Biochem.* **92**, 795–809.

Zhang X. F. and Forscher P. (2009) Rac1 modulates stimulus-evoked Ca2 + release in neuronal growth cones via parallel effects on microtubule/ER dynamics and ROS production. *Mol. Biol. Cell* **20**, 3700–3712.

